SLAC-PUB-972
(EXP)
October 1971

THE REACTION $\gamma p \rightarrow \rho^0 p$ AT 5.5 TO 18 GeV*

J. Park, M. Davier, I. Derado,** D. C. Fries,*** F. F. Liu,†
R. F. Mozley, A. C. Odian, W. P. Swanson, F. Villa, and D. Yount††

Stanford Linear Accelerator Center
Stanford University, Stanford, California 94305

ABSTRACT

The reaction $\gamma p \rightarrow \rho^0 p$ in the energy range $5.5 < E_\gamma < 18$ GeV was studied using a streamer chamber exposed to an 18 GeV bremsstrahlung beam. Our results differ from earlier counter experiments in the following ways: (1) the ρ cross section is constant (≈ 12 μb) throughout the energy range and (2) both $\frac{d\sigma}{dt}\Big|_{t_{min}}$ and the slope parameter of $\frac{d\sigma}{dt}$ are constant and have significantly smaller values (≈ 82 μb/GeV^2 and 6.6 GeV^{-2} respectively) at all of our energies. The t-dependence of the ρ density matrix in both s- and t-channel helicity frames shows that the production conserves the s-channel helicity at all t values observed (up to -0.8 GeV^2).

(Submitted to Nuclear Physics.)

(A preliminary report on the present data has been submitted to the International Symposium on Electron and Photon Interactions at High Energies, Cornell University, Ithaca, New York, August 23-27, 1971.)

---

*Work supported by the U. S. Atomic Energy Commission

**Max-Planck-Institute fur Physik und Astrophysik, Munich

***Institut fur Experimentale Kernphysik, Universitat Karlsruhe

†Physics Department, CSC-San Bernardino, California

††Department of Physics and Astronomy, University of Hawaii

In this report we present data for the photoproduction of ρ's in the reaction

$$\gamma p \rightarrow \rho^{o} p \qquad (1)$$

at photon energies in the range, 5.5 to 18 GeV.[1] Our current knowledge of this process at high energies derives mostly from the data of counter experiments.[2] The data described here are the first track-chamber data at energies above 9 GeV, and in particular the ρ decay information is new. The technique of the present experiment may be compared with previous work in the following respects: it shares many of the advantages of the bubble chamber technique (such as visual selection of topologies, and kinematic fitting), while extending the peak energy by a factor of 2, and with excellent sensitivity to small momentum recoil protons. Previous counter experiments fall into two categories: (1) those that detect the recoiling proton and (2) those that detect the pion pairs. Method (1) suffers from the lack of data at small t. Method (2) has the disadvantage of contamination from inelastic backgrounds.

We discuss the production and decay properties of ρ's as functions of the photon energy. Complementary aspects, namely, those as functions of the dipion mass have been described elsewhere.[3] Unlike results from counter experiments, we find: (1) the ρ production cross section is constant ($\approx 12\ \mu b$) throughout our energy range and (2) both $\left.\frac{d\sigma}{dt}\right|_{t_{min}}$ and the slope parameter of $\frac{d\sigma}{dt}$ are constant and have significantly smaller values ($\approx 82\ \mu b/GeV^2$ and $6.6\ GeV^{-2}$ respectively) at all of our energies. We determine the ρ density matrix at these energies in both s- and t-channel helicity frames, the t-dependence of which clearly shows that the reaction (1) conserves the s-channel helicity at all t values observed.

The data were obtained in a survey photoproduction experiment carried out at the Stanford Linear Accelerator Center using the 2-meter streamer chamber

with a pressurized hydrogen gas target exposed to an 18-GeV bremsstrahlung beam.[4] Measurements of 21,000 3-prong events (corresponding to 1/2 of the available data) yielded 5426 events for the process

$$\gamma p \rightarrow \pi^+ \pi^- p \qquad (2)$$

at all photon energies. The present report is based on 2147 events with the energy above 5.5 GeV.

The data were corrected (event-by-event) for the trigger and chamber efficiency by assigning a calculated weight to each event. The overall efficiency improves for higher energy. For our sample the average weight is 1.5 (corresponding to a combined efficiency of 67%) and only a small fraction (7% of total) have weights greater than 2. The use of a target tube (1/2-inch diameter, 4 mil thick mylar tube) made the vertex region invisible. This caused a scanning loss in detecting very low energy protons (which lose energy in the mylar) and high energy forward pions (which stay invisible for some distance away from the vertex). The effect is negligible for momentum transfers above 0.01 GeV^2. We estimate the overall loss due to this effect to be less than 10%.

Cross Sections

The cross sections for the process (2) are given in Table I for four different photon energy intervals. They are extracted from a subsample ($\approx$ 1/3 of the data reported here) with more restrictive fiducial volume cuts to minimize losses (discussed below) and for which the electron-positron pairs were measured to determine the beam energy spectrum. The number of equivalent quanta derived from this pair study was found to be in reasonable agreement with that monitored by the quantameter during the data taking run.

In order to obtain the cross sections, we have applied the following corrections to the data: (1) 15.8% owing to nonanalyzable events (excluding those with

obscuring flares in the chamber caused by steep tracks of the events), (2) 6.8% for misfiring of the chamber, and (3) 3.1% scanning loss due to the presence of pairs in the vertex region. In addition to the above energy independent corrections, the following energy dependent corrections (with magnitudes as given in Table I) were made: (4) loss due to the target tube including the effects of low energy protons (η_4) and high energy forward pions (η_5); (5) corrections due to untriggerable events (η_6).

Errors quoted for cross sections in Table I are statistical only. In addition to the energy dependent systematic errors ($\approx 4\%$) as given in the table, we estimate an overall systematic scale uncertainly of 8% in our results.

We note that, apart from the loss associated with small t (negligible above $|t| = 0.01$ GeV^2), the corrections to the normalization mentioned above do not affect the mass, momentum transfer and angular distributions (to be discussed below). These distributions are, of course, weighted ones to take into account (event-by-event) the nonideal trigger and chamber efficiency. Extensive studies[4] using a Monte Carlo technique were made to check that no distortions were introduced by the weighting.

Dipion Mass Spectra

As shown in the dipion mass distributions of Fig. 1 the reaction (2) at these energies is completely dominated by the production of ρ's. We have examined pion-nucleon mass distributions (not shown) and have found no significant structures including $\Delta^{++}(1236)$ at these energies.

The data in the mass region, $0.28 < m(\pi\pi) < 1.32$ GeV, were fitted using a simplified formulation of the Söding mechanism[5] in which the P-wave relativistic Breit-Wigner interferes coherently with the $\pi\pi$ diffraction scattering

amplitude (approximated by a pure imaginary constant)

$$\frac{\partial N}{\partial m} = C\left[\frac{m\, m_\rho \Gamma + \beta\left(m_\rho^2 - m^2\right)}{\left(m^2 - m_\rho^2\right)^2 + m_\rho^2 \Gamma^2} + B\right], \tag{3}$$

where

$$\Gamma = \Gamma_\rho \frac{m_\rho}{m}\left(\frac{m^2 - 4m_\pi^2}{m_\rho^2 - 4m_\pi^2}\right)^{3/2} .$$

The momentum dependence of the width causes the apparent shift of the ρ peak from a fitted value of 759 MeV to the observed value of 740 MeV and the interference term easily explains the skewness of the ρ shape as observed in the data. When all parameters of Eq. (3), namely, m_ρ, Γ_ρ, β, B and C, were freely varied in the fitting, the background term B tended toward unphysical (negative) values giving rise to widths which are larger than apparent in the data. Therefore in the final fit we took B to be identically zero. Results are summarized in Table II and are shown by curves in Fig. 1. For comparison we give in the table the corresponding results for the fraction of ρ (α_ρ in parentheses) from fitting an S-wave Breit-Wigner with invariant phase space. We note in particular that the fitted widths from the Söding model (average Γ_ρ = 118 MeV for m_ρ = 759 MeV) are somewhat narrower than apparent in the data. For instance, if we fit the mass spectra with the relativistic P-wave Breit-Wigner multiplied by the Ross and Stodolsky[6] factor $(m/m_\rho)^4$, then we obtain a larger width Γ_ρ = 140 ± 7 MeV (average on E_γ) for m_ρ = 762 ± 3 MeV with comparable χ^2.

As an attempt to remove the uncertainty in estimating the ρ cross section arising from the ambiguous ρ shape Yennie[7] has suggested measuring the $\pi\pi$

yield at the ρ mass from which one can determine the cross section as

$$\frac{d\sigma}{dt}(\gamma p \to \rho^o p) = \frac{\pi}{2}\,\Gamma_\rho\,\frac{d^2\sigma}{dtdm}(\gamma p \to \pi^+\pi^-)\Big|_{m=m_\rho}, \qquad (4)$$

since the contributions from Drell terms vanish at m_ρ. We use the integrated from

$$\sigma(\gamma p \to \rho^o p) = \frac{\pi}{2}\,\Gamma_\rho\,\frac{\Delta N}{\Delta m}\Big|_{m=m_\rho}\,\frac{1}{N}\,\sigma(\gamma p \to \pi^+\pi^- p). \qquad (5)$$

With the ρ parameters from an Orsay storage ring experiment,[8] $m_\rho = 780.2 \pm 5.9$ MeV and $\Gamma_\rho = 152.8 \pm 15.1$ MeV, and using the fitted values of $\Delta N/\Delta m$, we obtain the cross sections as given in Table III to be compared with those of Söding method. The two sets of values agree within 10%. Results do not differ by more than 10% if, instead of the above storage ring values, the nominal values,[9] $m_\rho = 765 \pm 10$ MeV, and $\Gamma_\rho = 125 \pm 20$ MeV, are used, since the effect of the narrower width is mostly compensated by the higher yield, $\Delta N/\Delta m$, at lower mass.

In Fig. 2 we compare our results (Söding method) with other experiments.[10] Bearing in mind the overall systematic scale uncertainty of 8% in our data and the additional theoretical uncertainty (due to the ambiguous ρ shape) of as much as 10%, our results are certainly consistent with those of Anderson et al.[13] (a counter experiment) above 12 GeV and agree well with the new bubble chamber result of Ballam et al.[12] (not shown) at 9 GeV, although they appear lower than others at lower energies.

From the above study of the dipion mass spectra, we conclude that in the ρ mass region of our data there is negligible background. In subsequent analysis we take as ρ events all events within the mass cut

$$0.62 < m(\pi\pi) < 0.86 \text{ GeV}. \qquad (6)$$

We emphasize that, since there is virtually no background, our results, such as the differential cross sections and decay angular distributions, are directly observable quantities and do not depend on model dependent calculations.

Differential Cross Sections

In Fig. 3 we show the differential cross sections for the reaction (1). These are obtained by normalizing the four-momentum transfer (t) distributions observed in the data with the mass cut (6) to corresponding total cross sections (Söding model) as given in Table III. The minimum, t, t_{min}, has been subtracted to remove the kinematic variation of t_{min} with the photon energy. The lines in Fig. 3 are results of the best fit of an exponential

$$A \exp\left[B(t-t_{min})\right] \tag{7}$$

to the data in the region $0.02 < |t-t_{min}| < 0.6$ GeV^2, excluding the data point below 0.02 GeV^2 owing to the possible scanning bias mentioned earlier. The forward cross sections $\frac{d\sigma}{dt}\Big|_{t_{min}}$ and slopes B thus obtained are listed in Table IV.

Our values for $\frac{d\sigma}{dt}\Big|_{t_{min}}$ as well as the exponential slope B agree well with the new bubble chamber result[11] at 9 GeV, but as shown in Fig. 4 they are significantly lower than the results of other experiments.[10] The discrepancy in $\frac{d\sigma}{dt}\Big|_{t_{min}}$ between our result and counter experiments ranges from 38% for $5.5 < E_\gamma < 7$ GeV to 15% for $12 < E_\gamma < 18$ GeV.

This discrepancy is largely due to the different methods of analysis used. In particular the forward cross sections of Anderson et al.[13] were obtained by fitting their data to a vector-dominance and quark model as follows

$$\frac{d\sigma}{dt}(\gamma p \to \rho p) = C_\rho \frac{d\sigma}{dt}(\gamma p \to \rho p) = C_\rho \left[\frac{1}{2}\sqrt{\frac{d\sigma}{dt}(\pi^+ p \to \pi^+ p)} + \frac{1}{2}\sqrt{\frac{d}{dt}(\pi^- p \to \pi^- p)}\right]^2 . \tag{8}$$

This model has one adjustable parameter C_ρ which is related to the conventional γ-ρ coupling constant as

$$C_\rho = \frac{1}{4}\alpha\frac{4\pi}{\gamma_\rho^2} \quad . \tag{9}$$

For comparison we have analyzed our data in the same manner. The data in the same t region as in the linear exponential case (7) were fitted to Eq. (8) allowing C_ρ to vary with energy. For πp elastic scattering we interpolated in energy the data of Foley et al.[14] using their parameterizations of total and differential cross sections. The results are summarized in Table IV and are shown by open circles in Fig. 3. Analyzed in a similar manner, our values for the forward cross section and the γ-ρ coupling constant agree well with those of Anderson et al. for $E_\gamma > 12$ GeV. However, the χ^2 of this fit is consistently worse than the linear exponential fit for each energy studied. This is hardly surprising since the πp elastic scattering has slope B around 9 GeV^{-2}, which is considerably higher than the apparent slope in our data of 6.6 GeV^{-2}.

Furthermore, in contrast to other experiments the forward cross section in our data is essentially constant in the entire energy range 5.5 to 18 GeV. These features in our data do not support the findings of other experiments in the same energy range that the vector dominance and quark model relating the πp elastic scattering to the forward ρ photoproduction give a satisfactory description.[15]

Decay Properties

We next turn to the decay properties of the ρ and present strong evidence in favor of s-channel helicity conservation.[16] In the rest frame of the ρ we introduce the two usual coordinate systems, called t-channel (Gottfried-Jackson) and s-channel helicity axes. The two systems are related to each other by a rotation about the common y-axis, which is chosen normal to the ρ production plane. In

the t-channel helicity system the z-axis is taken along the photon direction in the ρ rest frame, whereas in the s-channel helicity frame it is defined to be along the direction of ρ in the overall center-of-mass. Using the π^+ as an analyzer we then consider the polar and azimuthal angles with respect to each of the two coordinate systems.

In Fig. 5 we show the projected angular distributions of events in the ρ region defined by the mass cut $0.62 < m(\pi\pi) < 0.86$ GeV. The subscript H (J) refers to the s-channel (t-channel) helicity system. Assuming a pure $J^P = 1^-$ decay (conserving parity) into two pseudoscalars, we expect that the form of the angular distribution in either system is

$$\frac{\partial W}{\partial \Omega} = \frac{3}{4\pi}\left[\rho_{00}\cos^2\theta + \rho_{11}\sin^2\theta - \rho_{1-1}\sin^2\theta\cos^2\phi - \sqrt{2}\,(\mathrm{Re}\,\rho_{10})\sin^2\theta\cos\phi\right] \tag{10}$$

The curves in Fig. 3 are results of a best fit of Eq. (10) to projected distributions. These results, including the density matrix elements, are also given in Table V. We find the overall results to be satisfactory so that our treatment of the data in the ρ mass region without background appears reasonable.

We have also carried out a moment analysis of the data in this mass region to study the momentum transfer dependence of the density matrix elements. Again assuming a pure vector meson decay we have in either coordinate systems[17]

$$\begin{aligned}
\rho_{11} = \rho_{-1-1} &= \frac{1}{3} - \frac{\sqrt{5}}{6}\langle Y_{20}/Y_{00}\rangle \ , \\
\rho_{1-1} = \rho_{-11} &= -\sqrt{\frac{5}{6}}\ \mathrm{Re}\,\langle Y_{22}/Y_{00}\rangle \ , \\
\mathrm{Re}\,\rho_{01} = \mathrm{Re}\,\rho_{10} &= -\mathrm{Re}\,\rho_{0-1} = -\mathrm{Re}\,\rho_{-10} = \sqrt{\frac{5}{12}}\ \mathrm{Re}\,\langle Y_{21}/Y_{00}\rangle \ .
\end{aligned} \tag{11}$$

The moments in Eq. (11) are obtained according to

$$\langle Y_{LM} \rangle = \sum_i w_i Y_{LM}(\Omega_i) / \sum w_i$$

where w_i is the weight for ith event. Corresponding errors are estimated as

$$\delta \langle Y_{LM}/Y_{00} \rangle = \left[\sum w_i \left(Y_{LM}\right)^2 - \left(\sum w_i Y_{LM}\right)^2 / \sum w_i \right]^{1/2} / \left(\sum w_i Y_{00}\right) .$$

The results including the observed moments are summarized in Table VI. As seen in the table the density matrix takes the simplest form, $\rho_{11} = \rho_{-1-1} = \frac{1}{2}$ and all others = 0, in the s-channel helicity frame. We find this to be true for all momentum transfer values observed and at all photon energies studied. In Fig. 4 we compare the behavior of ρ_{11} in the s-channel frame with ρ_{11} in the t-channel as a function of momentum transfer. It clearly shows that the data prefer the s-channel helicity conservation over the t-channel helicity nonflip.

We wish to acknowledge helpful discussions with members of the SLAC-Berkeley-Tuft collaboration and thank Leroy Schwarcz, our engineers, technicians, programmers and scanners for their many contributions.

REFERENCES

1. A preliminary report on the present data has been submitted to the International Symposium on Electron and Photon Interactions at High Energies (1971), Ithaca, New York.
2. See, for instance, P. Joos, "Compilation of photoproduction data above 1.2 GeV," Report No. DESY-HERA 70-1 (1970).
3. J. Park, "The reaction $\gamma p \rightarrow \pi^+\pi^- p$ at 5.5 to 18 GeV and a dual resonance model," Report No. SLAC-PUB-971 (1971) (to be published).
4. This is the second photoproduction experiment using the streamer chamber at SLAC. The experimental technique was similar to the first one which has been described in Ref. 11. A detailed report on the experimental arrangement and the data analysis of the present experiment is in preparation.
5. P. Söding, Phys. Rev. Letters 19, 702 (1966).
6. M. Ross and L. Stodolsky, Phys. Rev. 149, 1172 (1966).
7. See, for instance, the related discussions in J. Ballam et al., "Bubble chamber study of photoproduction by 2.8 and 4.7 GeV polarized photons, Report No. SLAC-PUB-941 (1971).
8. J. Lefrancois, "Results of the Orsay Storage Ring A.C.O." submitted to the International Symposium on Electron and Photon Interactions at High Energies (1971), Ithaca, New York.
9. Particle Data Group, "Review of particle properties," Rev. Mod. Phys. 43, No. 2, Part II (1971).
10. Figures 2 and 4 are prepared from the compilation of P. Joos (Ref. 2) and do not include the new bubble chamber result (Ref. 12). In the figure SLAC/B (68) refers to J. Ballam et al., Phys. Rev. Letters 21, 1541 (1968); SLAC/B (69) to J. Ballam et al., Phys. Letters 30B, 421 (1969); DESY (69)

to ABBHHM collaboration, Phys. Rev. 175, 1669 (1969); Cornell (69) to K. Gottfried et al., Phys. Rev. Letters 22, 374 (1969); DESY-MIT to H. Alvensleben et al., Phys. Rev. Letters 23, 1058 (1969); SLAC/F (68) to W. G. Jones et al., Phys. Rev. Letters 21, 586 (1968); SLAC/F (70) to Ref. 13 and SLAC/D (69) to Ref. 11.

11. M. Davier et al., Phys. Rev. D1, 790 (1970).

12. J. Ballam et al., "A Study of the Channel $\gamma p \rightarrow p\pi^+\pi^-$ Using a Linearly Polarized Photon Beam of Energy 9.3 GeV," submitted to the International Symposium on Electron and Photon Interactions at High Energies (1971), Ithaca, New York. This report contains (1) the ρ cross section $\sigma(\mu b) = 12.4 \pm 0.5$ to 13.1 ± 0.6, (2) the forward cross section $d\sigma/dt\ (\mu b/GeV^2) = 79 \pm 4$ to 90 ± 5 and (3) the exponential slope $A(GeV^{-2}) = 6.6 \pm 0.3$ to 7.1 ± 0.3 depending on models used.

13. R. Anderson et al., Phys. Rev. D1, 27 (1970).

14. K. J. Foley et al., Phys. Rev. Letters 11, 425 (1963).

15. See, for instance, separate reviews by G. Kramer and R. Marshall, "Vector Meson Production and Omega-Rho Interference," Proceedings of the Daresbury Study Weekend, 12-14 June, 1970, edited by A. Donachie and E. Gabathnler, Daresbury Nuclear Physics Laboratory.

16. Proposed by F. J. Gilman et al., Phys. Letters 31B, 387 (1970) and confirmed by J. Ballam et al., Phys. Rev. Letters 24, 960 (1970) in the photoproduction of ρ at 2.8 and 4.7 GeV.

17. For general formalism see the lecture by J. D. Jackson in High Energy Physics, edited by C. DeWitt and M. Jacob (Gordon and Breach Science Publishers Inc., New York, 1966).

Table I. Cross sections for $\gamma p \rightarrow \pi^+ \pi^- p$

E_γ (GeV)	X_V(m) [a]	N [b]	$\sum w_i$ [c]	η_4 (%) [d]	η_5 (%)	η_6 (%)	$\delta\eta$ (%) [e]	C [f]	σ (μb) [g]
5.5 - 7	0.15 - 1.25	178	270.4	5.2	0.0	3.7	3.4	1.441	15.41 ± 1.18
5 - 9	0.15 - 1.05	137	209.6	2.8	2.4	2.9	2.8	1.428	15.05 ± 1.32
9 - 12	0.15 - 1.05	132	200.5	4.6	5.6	4.3	3.4	1.527	14.35 ± 1.28
12 - 18	0.15 - 1.05	161	255.0	9.4	8.7	4.7	4.4	1.667	14.37 ± 1.17

[a] Vertex coordinate along the beam direction.

[b] Raw number of events.

[c] Weight for each event to account for nonideal trigger and chamber efficiency.

[d] η_4, η_5, and η_6 are energy dependent corrections to the data as discussed in the text.

[e] Energy dependent systematic errors. In addition there is an overall systematic scale uncertainty of 8%. Estimates are made based on the size and type of corrections needed.

[f] Overall correction factor including the total energy independent correction of 23.9%.

[g] Errors quoted are statistical only and do not include systematic uncertainty (see the remark e above).

Table II. Fit of dipion mass distribution in $\gamma p \rightarrow p\ \pi^+\pi^-$

E_γ (GeV)	m_ρ (GeV)	Γ_ρ (GeV)	β	χ^2/ndf	α_ρ (%)
5.5 - 7	0.756 ± 0.004	0.119 ± 0.006	0.20 ± 0.02	103/22	79.7(81)
7 - 9	0.762 ± 0.004	0.113 ± 0.006	0.21 ± 0.02	42/21	80.6(82)
9 - 12	0.766 ± 0.004	0.114 ± 0.006	0.28 ± 0.02	76/20	81.4(82)
12 - 18	0.751 ± 0.005	0.125 ± 0.006	0.19 ± 0.02	143/21	81.0(83)

Table III. Cross sections for $\gamma p \rightarrow \rho^o p$

	Söding Method		Yennie Method	
E_γ (GeV)	α_ρ (%)	$\sigma(\mu b)$ [(a)]	α_ρ (%)	$\sigma(\mu b)$ [(b)]
5.5 - 7	79.7	12.3 ± 0.9	76.9	11.8 ± 1.5
7 - 9	80.6	12.1 ± 1.1	87.6	13.2 ± 1.7
9 - 12	81.4	11.7 ± 1.0	90.2	13.0 ± 1.6
12 - 18	81.0	11.6 ± 1.0	69.3	10.0 ± 1.3

(a) The quoted error is due only to the statistical error of $\sigma(\gamma p \rightarrow p\pi^+\pi^-)$ as given in Table I.

(b) The quoted error is due only to statistics and does not include systematic effects in the data and uncertainties in the ρ-parameters.

Table IV. Fit of differential cross sections for $\gamma p \rightarrow \rho^o p$

E_γ (GeV)	Exponential Fit			VDM and Quark Model Fit		
	χ^2/ndf	$\frac{d\sigma}{dt}\Big\|_{t_{min}} \left[\frac{\mu b}{GeV^2}\right]$	B $(GeV)^{-2}$	χ^2/ndf	$\frac{d\sigma}{dt}\Big\|_{t_{min}} \left[\frac{\mu b}{GeV^2}\right]$	$\gamma_\rho^2/4\pi$
5.5 - 7	53/27	82.6 ± 6.5	6.4 ± 0.4	82/28	114.5 ± 5.5	0.82 ± 0.04
7 - 9	30/27	79.6 ± 6.3	6.5 ± 0.4	46/28	105.6 ± 5.1	0.76 ± 0.04
9 - 12	22/27	75.5 ± 6.0	6.1 ± 0.4	53/28	106.7 ± 5.2	0.70 ± 0.03
12 - 18	49/27	90.1 ± 6.4	7.2 ± 0.4	65/28	112.2 ± 6.5	0.62 ± 0.04

Table V. Density matrix elements from least square fit of projected distributions

E_γ (GeV)	s-channel helicity system				t-channel helicity system			
	χ^2/ndf	ρ_{11}	χ^2/ndf	ρ_{1-1}	χ^2/ndf	ρ_{11}	χ^2/ndf	ρ_{1-1}
5.5 - 7	22/18	0.507 ± 0.011	27/22	0.053 ± 0.032	48/18	0.353 ± 0.017	39/22	0.218 ± 0.032
7 - 9	22/18	0.473 ± 0.014	50/22	0.028 ± 0.031	27/18	0.326 ± 0.018	26/22	0.148 ± 0.032
9 - 12	36/18	0.502 ± 0.012	17/22	-0.097 ± 0.033	15/18	0.296 ± 0.018	49/22	0.109 ± 0.033
12 - 18	22/18	0.506 ± 0.011	36/22	-0.020 ± 0.030	22/18	0.329 ± 0.016	19/22	0.128 ± 0.030

Table VI. ρ Density Matrix Elements for $\gamma p \rightarrow \rho^{o} p$

$5.5 < E_{\gamma} < 7$ GeV

S-CHANNEL HELICITY SYSTEM

-T+T(MIN)	<Y20/Y00>	<RE Y21/Y00>	<RE Y22/Y00>	RHO(11)	RE RHO(01)	RHO(1-1)
0.00-0.04	-0.520+-0.070	-0.001+-0.074	0.023+-0.087	0.527+-0.026	-0.001+-0.048	-0.021+-0.080
0.04-0.08	-0.638+-0.060	0.153+-0.057	-0.101+-0.091	0.571+-0.022	0.099+-0.037	0.093+-0.083
0.08-0.12	-0.388+-0.083	0.013+-0.074	-0.015+-0.085	0.478+-0.031	0.008+-0.048	0.013+-0.077
0.12-0.20	-0.513+-0.065	-0.095+-0.055	-0.101+-0.076	0.525+-0.024	-0.061+-0.036	0.092+-0.069
0.20-0.40	-0.486+-0.063	0.140+-0.064	-0.014+-0.082	0.514+-0.023	0.090+-0.041	0.013+-0.075
>0.40	-0.432+-0.144	0.133+-0.094	0.015+-0.143	0.494+-0.054	0.086+-0.060	-0.014+-0.130
ALL	-0.504+-0.030	0.044+-0.028	-0.042+-0.036	0.521+-0.011	0.028+-0.018	0.039+-0.033

T-CHANNEL HELICITY SYSTEM

-T+T(MIN)	<Y20/Y00>	<RE Y21/Y00>	<RE Y22/Y00>	RHO(11)	RE RHO(01)	RHO(1-1)
0.00-0.04	-0.424+-0.082	0.233+-0.070	-0.016+-0.084	0.491+-0.031	0.151+-0.045	0.014+-0.077
0.04-0.08	-0.137+-0.093	0.366+-0.059	-0.306+-0.074	0.384+-0.035	0.236+-0.038	0.279+-0.068
0.08-0.12	-0.057+-0.104	0.248+-0.066	-0.149+-0.079	0.355+-0.039	0.160+-0.042	0.136+-0.072
0.12-0.20	-0.147+-0.091	0.271+-0.054	-0.250+-0.063	0.388+-0.034	0.175+-0.035	0.228+-0.057
0.20-0.40	0.300+-0.114	0.083+-0.057	-0.335+-0.052	0.221+-0.043	0.054+-0.037	0.306+-0.048
>0.40	0.206+-0.192	-0.107+-0.102	-0.245+-0.106	0.257+-0.072	-0.069+-0.066	0.224+-0.097
ALL	-0.060+-0.045	0.215+-0.027	-0.224+-0.030	0.356+-0.017	0.139+-0.017	0.204+-0.028

Table VI(cont'd) - 2

$7 < E_\gamma < 9$

S-CHANNEL HELICITY SYSTEM

-T+T(MIN)	<Y20/Y00>	<RE Y21/Y00>	<RE Y22/Y00>	RHO(11)	RE RHO(01)	RHO(1-1)
0.00-0.04	-0.374+-0.076	0.126+-0.072	-0.145+-0.078	0.473+-0.028	0.081+-0.047	0.132+-0.072
0.04-0.08	-0.203+-0.099	-0.045+-0.070	-0.127+-0.078	0.409+-0.037	-0.029+-0.045	0.116+-0.071
0.08-0.12	-0.364+-0.081	-0.083+-0.089	0.116+-0.083	0.469+-0.030	-0.053+-0.057	-0.106+-0.076
0.12-0.20	-0.487+-0.082	-0.061+-0.074	0.114+-0.090	0.515+-0.031	-0.040+-0.048	-0.104+-0.082
0.20-0.40	-0.430+-0.076	-0.050+-0.063	-0.016+-0.086	0.494+-0.028	-0.032+-0.041	0.015+-0.078
>0.40	0.159+-0.129	-0.058+-0.079	0.110+-0.084	0.274+-0.048	-0.038+-0.051	-0.100+-0.077
ALL	-0.298+-0.038	-0.023+-0.030	-0.003+-0.034	0.445+-0.014	-0.015+-0.020	0.003+-0.031

T-CHANNEL HELICITY SYSTEM

-T+T(MIN)	<Y20/Y00>	<RE Y21/Y00>	<RE Y22/Y00>	RHO(11)	RE RHO(01)	RHO(1-1)
0.00-0.04	-0.199+-0.110	0.213+-0.048	-0.216+-0.077	0.408+-0.041	0.138+-0.031	0.197+-0.070
0.04-0.08	-0.184+-0.100	0.050+-0.070	-0.134+-0.078	0.402+-0.037	0.032+-0.045	0.123+-0.071
0.08-0.12	-0.090+-0.113	0.295+-0.064	0.004+-0.086	0.367+-0.042	0.190+-0.041	-0.004+-0.079
0.12-0.20	0.058+-0.107	0.320+-0.073	-0.108+-0.079	0.312+-0.040	0.206+-0.047	0.099+-0.072
0.20-0.40	0.139+-0.110	0.199+-0.061	-0.249+-0.065	0.281+-0.041	0.129+-0.040	0.227+-0.059
>0.40	0.451+-0.125	0.219+-0.088	-0.010+-0.066	0.165+-0.047	0.141+-0.057	0.009+-0.060
ALL	0.012+-0.046	0.212+-0.027	-0.130+-0.031	0.329+-0.017	0.137+-0.018	0.118+-0.029

Table VI(cont'd) - 3

$9 < E_\gamma < 12$

S-CHANNEL HELICITY SYSTEM

-T+T(MIN)	<Y20/Y00>	<RE Y21/Y00>	<RE Y22/Y00>	RHO(11)	RE RHO(01)	RHO(1-1)
0.00-0.04	-0.400+-0.083	-0.045+-0.087	0.213+-0.104	0.482+-0.031	-0.029+-0.056	-0.194+-0.095
0.04-0.08	-0.262+-0.091	0.162+-0.084	0.115+-0.083	0.431+-0.034	0.105+-0.054	-0.105+-0.076
0.08-0.12	-0.478+-0.085	0.004+-0.076	0.032+-0.092	0.512+-0.032	0.003+-0.049	-0.029+-0.084
0.12-0.20	-0.442+-0.077	0.157+-0.067	0.111+-0.082	0.498+-0.029	0.102+-0.043	-0.101+-0.075
0.20-0.40	-0.537+-0.061	0.054+-0.064	0.034+-0.066	0.534+-0.023	0.035+-0.041	-0.031+-0.061
>0.40	-0.531+-0.113	0.074+-0.095	0.176+-0.140	0.531+-0.042	0.048+-0.062	-0.161+-0.128
ALL	-0.438+-0.034	0.074+-0.032	0.103+-0.036	0.496+-0.013	0.048+-0.021	-0.094+-0.033

T-CHANNEL HELICITY SYSTEM

-T+T(MIN)	<Y20/Y00>	<RE Y21/Y00>	<RE Y22/Y00>	RHO(11)	RE RHO(01)	RHO(1-1)
0.00-0.04	-0.318+-0.098	0.219+-0.083	0.180+-0.100	0.452+-0.037	0.141+-0.054	-0.164+-0.091
0.04-0.08	0.101+-0.127	0.263+-0.065	-0.033+-0.076	0.296+-0.047	0.170+-0.042	0.030+-0.069
0.08-0.12	-0.104+-0.112	0.295+-0.069	-0.121+-0.083	0.372+-0.042	0.190+-0.044	0.110+-0.076
0.12-0.20	0.276+-0.108	0.241+-0.067	-0.182+-0.063	0.230+-0.040	0.156+-0.043	0.166+-0.057
0.20-0.40	0.219+-0.092	0.177+-0.061	-0.275+-0.050	0.252+-0.034	0.114+-0.039	0.251+-0.046
>0.40	0.506+-0.196	-0.019+-0.094	-0.247+-0.082	0.145+-0.073	-0.012+-0.061	0.225+-0.075
ALL	0.100+-0.048	0.216+-0.029	-0.116+-0.031	0.296+-0.018	0.139+-0.019	0.106+-0.029

Table VI(cont'd) - 4

$12 < E_\gamma < 18$

S-CHANNEL HELICITY SYSTEM

-T+T(MIN)	<Y20/Y00>	<RE Y21/Y00>	<RE Y22/Y00>	RHO(11)	RE RHO(01)	RHO(1-1)
0.00-0.04	-0.487+-0.065	0.006+-0.064	0.039+-0.080	0.515+-0.024	0.004+-0.041	-0.036+-0.073
0.04-0.08	-0.602+-0.054	0.030+-0.058	-0.101+-0.077	0.558+-0.020	0.019+-0.037	0.092+-0.070
0.08-0.12	-0.427+-0.072	0.136+-0.074	0.199+-0.082	0.492+-0.027	0.088+-0.047	-0.182+-0.075
0.12-0.20	-0.391+-0.073	0.070+-0.059	0.067+-0.068	0.479+-0.027	0.045+-0.038	-0.062+-0.062
0.20-0.40	-0.391+-0.067	0.054+-0.066	0.106+-0.075	0.479+-0.025	0.035+-0.042	-0.097+-0.068
>0.40	-0.363+-0.138	-0.103+-0.105	-0.329+-0.117	0.469+-0.051	-0.066+-0.068	0.300+-0.107
ALL	-0.451+-0.030	0.048+-0.028	0.038+-0.033	0.501+-0.011	0.031+-0.018	-0.035+-0.030

T-CHANNEL HELICITY SYSTEM

-T+T(MIN)	<Y20/Y00>	<RE Y21/Y00>	<RE Y22/Y00>	RHO(11)	RE RHO(01)	RHO(1-1)
0.00-0.04	-0.311+-0.072	0.244+-0.064	-0.033+-0.078	0.449+-0.027	0.157+-0.041	0.030+-0.071
0.04-0.08	-0.275+-0.084	0.302+-0.051	-0.234+-0.068	0.436+-0.031	0.195+-0.033	0.214+-0.062
0.08-0.12	0.167+-0.100	0.347+-0.069	-0.043+-0.072	0.271+-0.037	0.224+-0.044	0.040+-0.066
0.12-0.20	0.175+-0.088	0.217+-0.061	-0.163+-0.056	0.268+-0.033	0.140+-0.039	0.149+-0.051
0.20-0.40	0.287+-0.100	0.140+-0.061	-0.171+-0.059	0.226+-0.037	0.090+-0.039	0.156+-0.054
>0.40	-0.187+-0.156	0.105+-0.099	-0.400+-0.111	0.403+-0.058	0.068+-0.064	0.365+-0.101
ALL	0.004+-0.040	0.235+-0.027	-0.147+-0.029	0.332+-0.015	0.152+-0.017	0.134+-0.026

FIGURE CAPTIONS

1. Dipion mass distributions in $\gamma p \rightarrow \pi^+ \pi^- p$ for several photon energy intervals. Distributions have been weighted to correct for trigger and chamber efficiency. Numbers in parentheses refer to unweighted events. Curves are results of a best fit of the Söding model as described in the text.
2. Compilation of $\sigma(\gamma p \rightarrow \rho p)$ for $E_\gamma > 5$ GeV. See footnote 9 for references.
3. Differential cross sections for $\gamma p \rightarrow \rho^0 p$ obtained by normalizing each momentum transfer distribution observed in the mass region $0.62 < m(\pi\pi) < 0.86$ GeV to the measured total cross section. Lines (open circles) show results of a best fit of an exponential (vector-dominance and quark model) excluding the first data point for possible scanning bias.
4. Compilation of the forward ρ cross section for $E_\gamma > 5$ GeV. See footnote 9 for references.
5. Decay angular distributions of the ρ^0 in $\gamma p \rightarrow \rho^0 p$. Subscript H(J) refers to the s-channel (t-channel) helicity system. All events in the mass region, $0.62 < m(\pi\pi) < 0.86$ GeV are taken as ρ events. Curves show expected forms assuming a pure vector meson decay.
6. Behavior of the density matrix element ρ_{11} of the ρ^0 in $\gamma p \rightarrow \rho^0 p$ as a function of the momentum transfer in both s- and t-channel helicity frames. The data clearly supports the s-channel helicity conservation as opposed to the t-channel helicity nonflip.

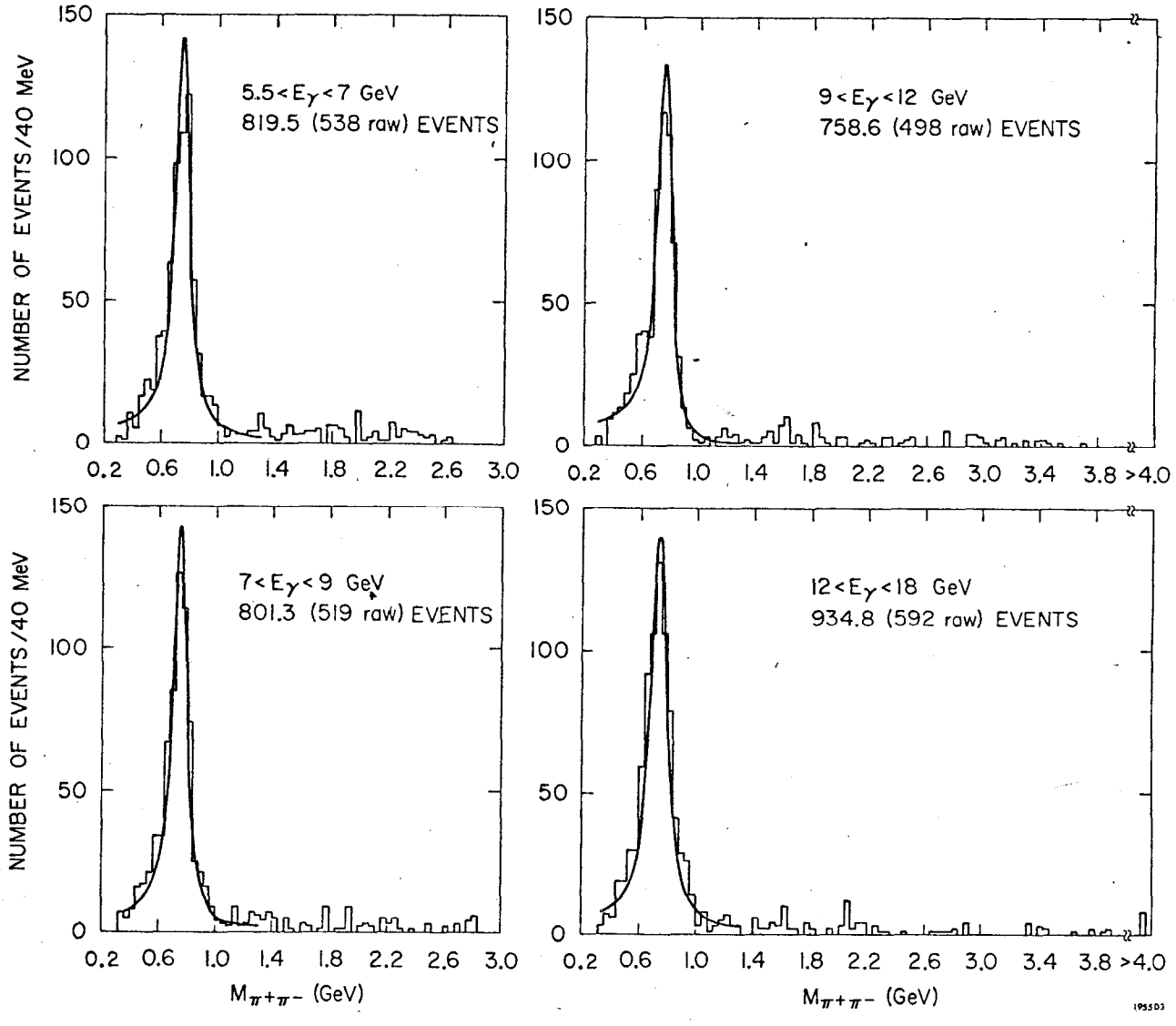
NUMBER OF EVENTS/40 MeV
150
100
50
0
5.5<Eγ<7 GeV
819.5 (538 raw) EVENTS
9<Eγ<12 GeV
758.6 (498 raw) EVENTS
7<Eγ<9 GeV
801.3 (519 raw) EVENTS
12<Eγ<18 GeV
934.8 (592 raw) EVENTS
0.2 0.6 1.0 1.4 1.8 2.2 2.6 3.0 3.4 3.8 >4.0
Mπ+π− (GeV)
19550-3

Fig. 1

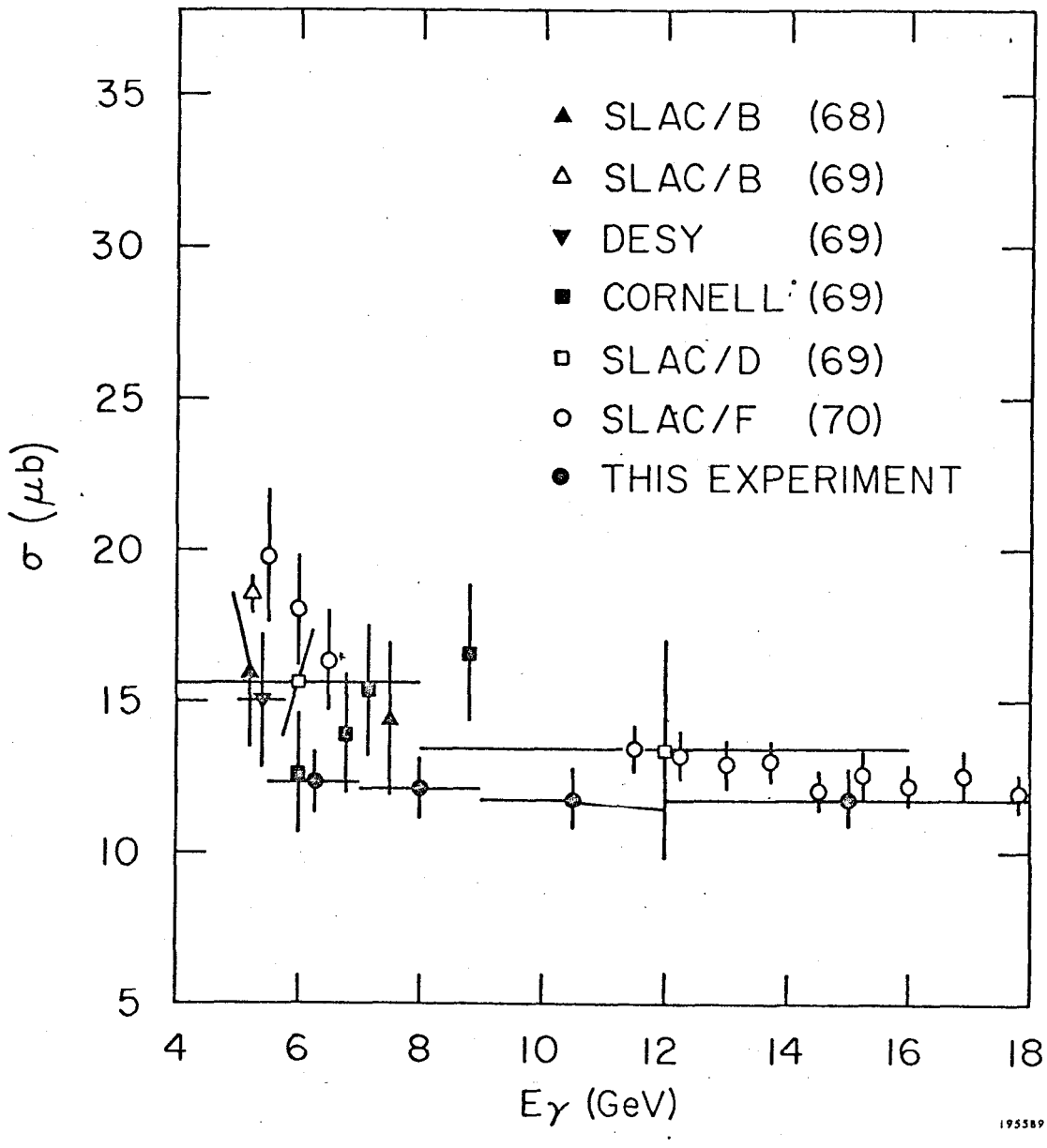
35
30
25
20
15
10
5
σ (μb)
4
6
8
10
12
14
16
18
Eγ (GeV)
SLAC/B (68)
SLAC/B (69)
DESY (69)
CORNELL (69)
SLAC/D (69)
SLAC/F (70)
THIS EXPERIMENT
195589

Fig. 2

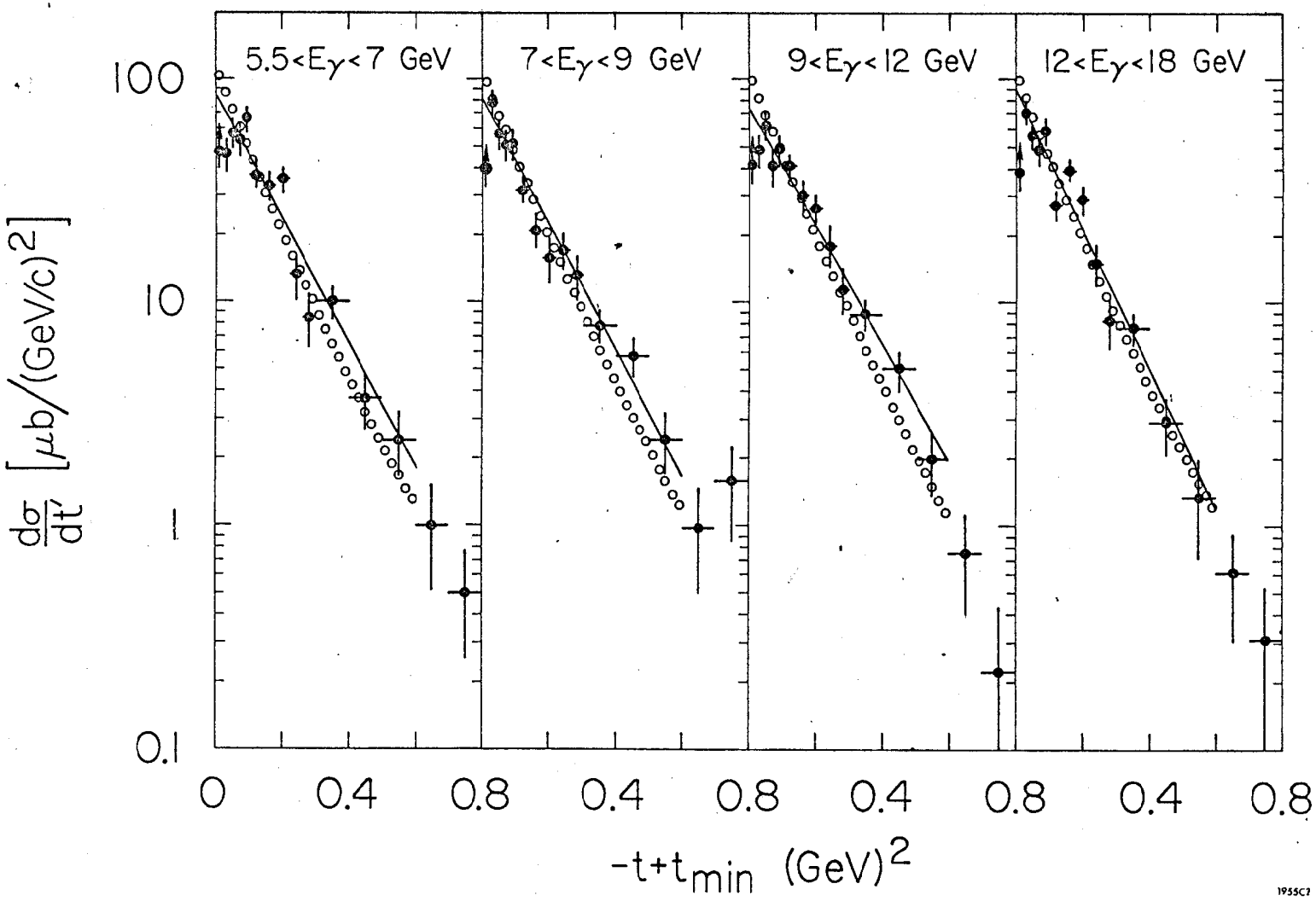
5.5<Eγ<7 GeV
7<Eγ<9 GeV
9<Eγ<12 GeV
12<Eγ<18 GeV
100
10
1
0.1
0
0.4
0.8
dσ/dt' [μb/(GeV/c)²]
-t+t_min (GeV)²
1955C7

Fig. 3

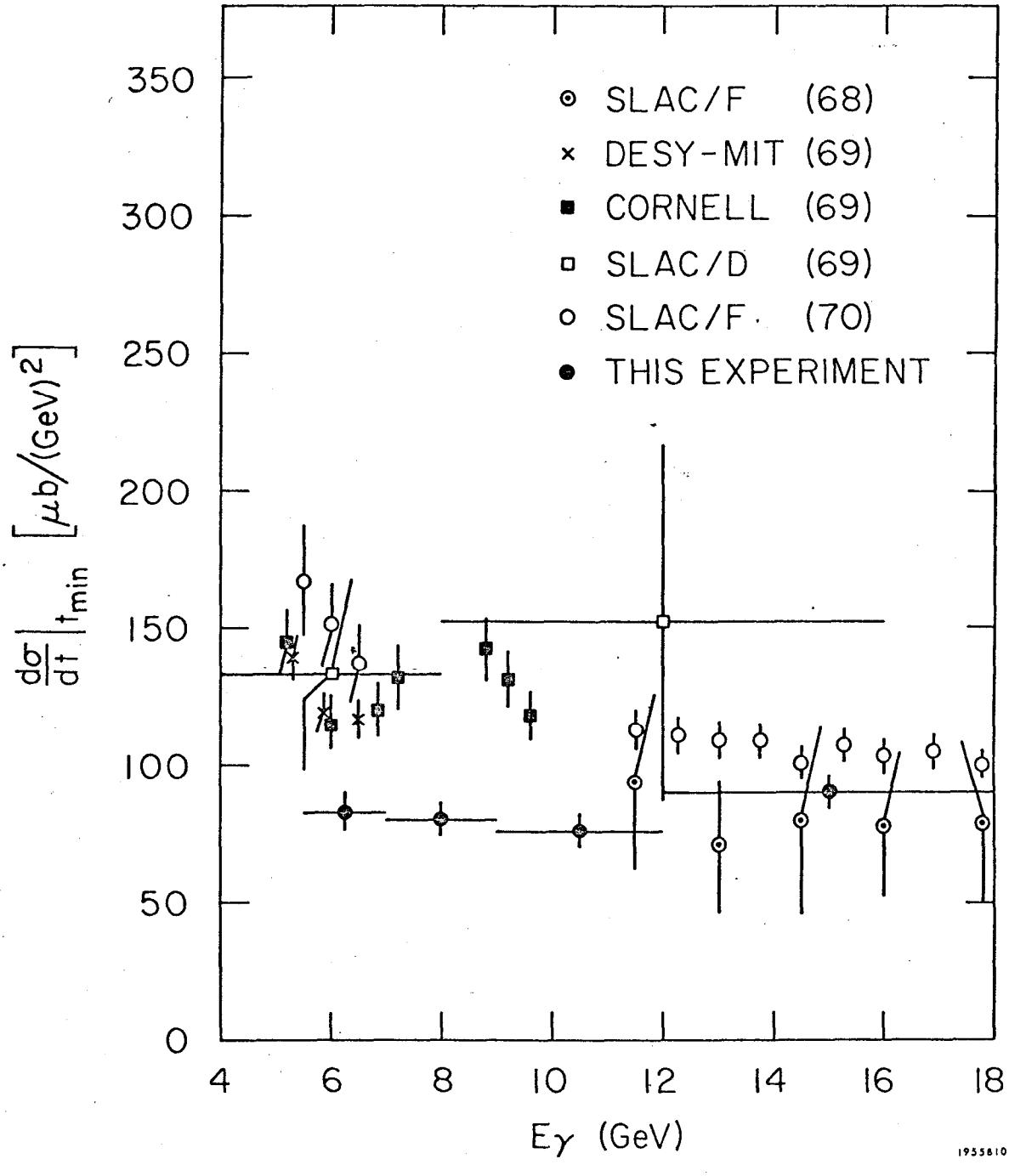
SLAC/F (68)
DESY-MIT (69)
CORNELL (69)
SLAC/D (69)
SLAC/F (70)
THIS EXPERIMENT
$\frac{d\sigma}{dt}\Big|_{t_{min}}$ [μb/(GeV)^2]
350
300
250
200
150
100
50
0
4
6
8
10
12
14
16
18
E_γ (GeV)
1955810

Fig. 4

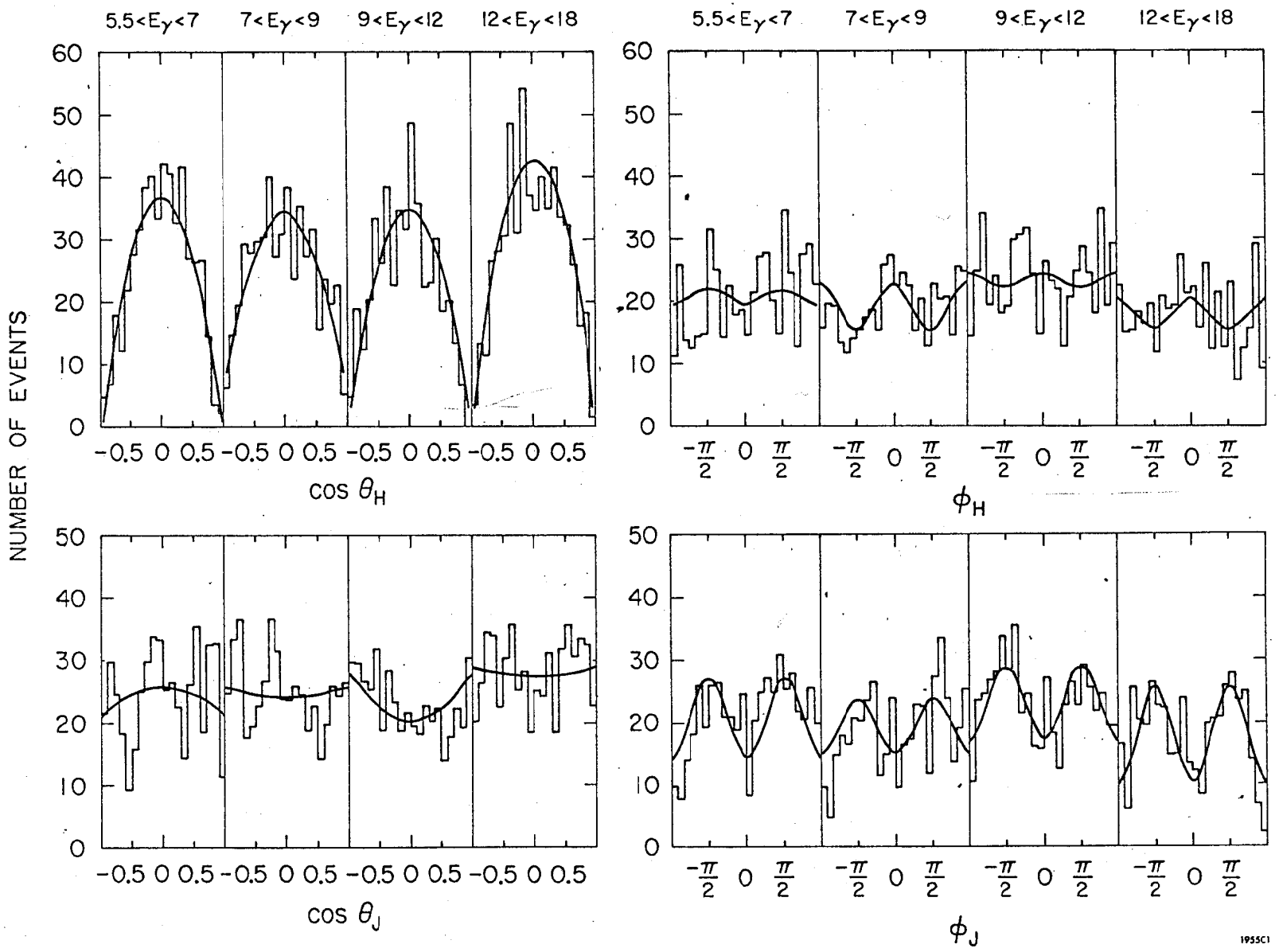
5.5<Eγ<7
7<Eγ<9
9<Eγ<12
12<Eγ<18
NUMBER OF EVENTS
cos θH
φH
cos θJ
φJ
1955C1

Fig. 5

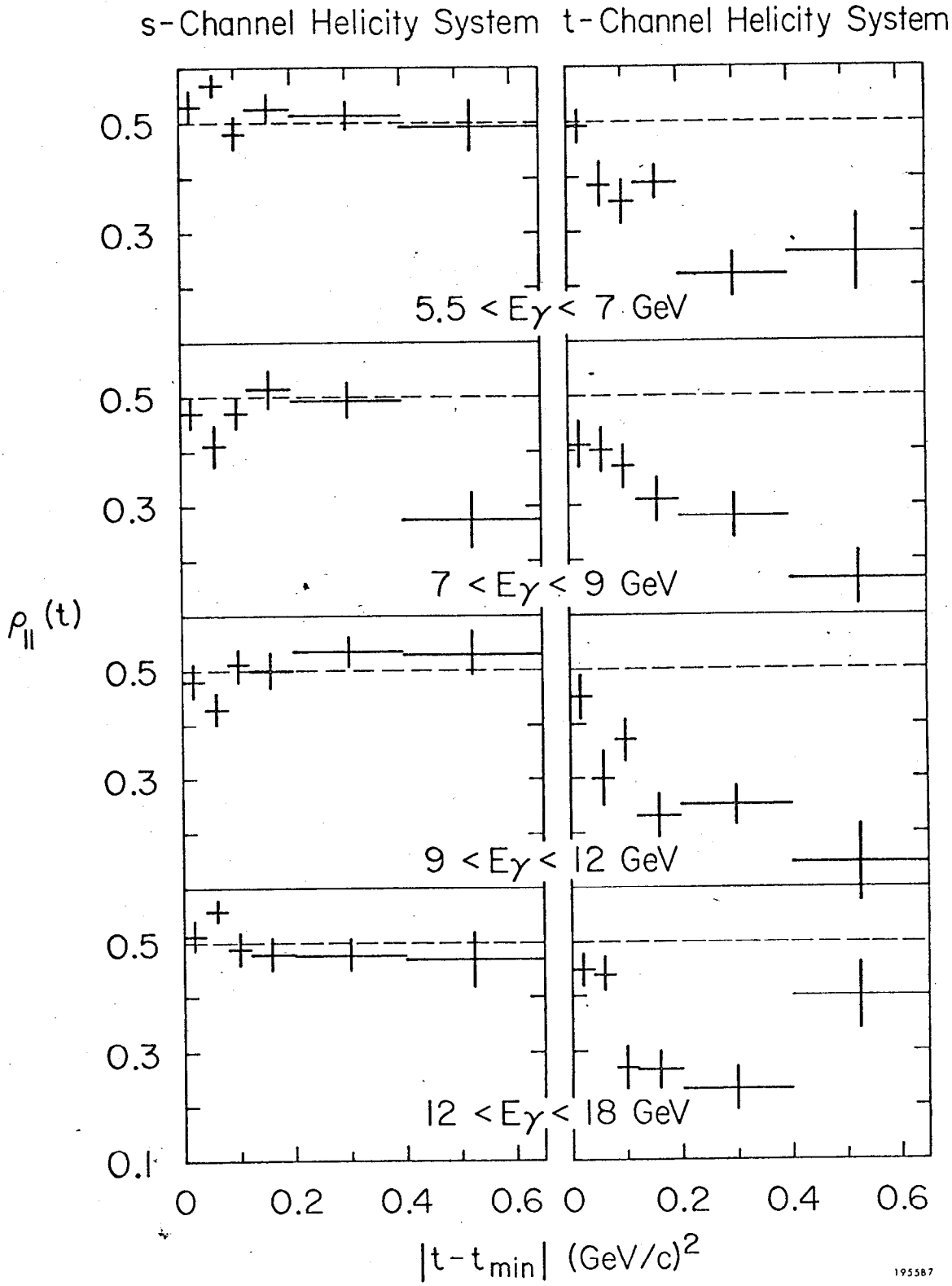
s-Channel Helicity System
t-Channel Helicity System
$\rho_{11}(t)$
0.5
0.3
0.1
5.5 < Eγ < 7 GeV
7 < Eγ < 9 GeV
9 < Eγ < 12 GeV
12 < Eγ < 18 GeV
0
0.2
0.4
0.6
$|t-t_{min}|$ (GeV/c)^2
1955B7

Fig. 6